Journal of Zhejiang University-SCIENCE A (Applied Physics & Engineering) 2023 24(3):272-283
www.jzus.zju.edu.cn; www.springer.com/journal/11582
E-mail: jzus_a@zju.edu.cn

Research Article

https://doi.org/10.1631/jzus.A2200189

Adaptive fault-tolerant control of high-speed maglev train suspension system with partial actuator failure: design and experiments

Yougang SUN[1,2], Fengxing LI[1], Guobin LIN[2], Junqi XU[2]✉, Zhenyu HE[1]

[1]*Institute of Rail Transit, Tongji University, Shanghai 201804, China*
[2]*National Maglev Transportation Engineering R&D Center, Tongji University, Shanghai 201804, China*

Abstract: High-speed maglev trains will play an important role in the high-speed transportation system in the near future. However, under the conditions of strong magnetic fields and continuous operation, the actuators of the high-speed maglev train suspension system are prone to lose partial effectiveness, which makes the suspension control problem challenging. In addition, most existing fault-tolerant control (FTC) methods for suspension systems require linearization around the equilibrium points during the controller design or stability analysis. Therefore, from a practical perspective, this study presents a novel nonlinear FTC strategy with adaptive compensation for high-speed maglev train suspension systems. First, a nonlinear dynamic model of the suspension system based on join-structure is established and the actuator failures are described. Then, a nonlinear fault-tolerant suspension control law with an adaptive update law is designed to achieve stable suspension against partial actuator failure. The Lyapunov theory and extended Barbalat lemma are utilized to rigorously prove the closed-loop asymptotic stability even if there is partial actuator failure, without any approximation to the original nonlinear dynamics. Finally, hardware experimental results are included to demonstrate the effectiveness of the proposed approach.

Key words: High-speed maglev transportation; Suspension control system; Adaptive fault-tolerant control (FTC); Partial actuator failure; Mechatronics

1 Introduction

High-speed maglev transport relies on its high-speed domain, fast acceleration and deceleration, strong climbing capacity, and economical operation and maintenance, to fill the speed gap between traditional wheel-track high speed rail and air transport (Lee et al., 2006; Fang and Yao, 2007; Boldea et al., 2018). In 2021, China's "National Comprehensive Three-Dimensional Transportation Network Planning Outline" pointed out that 600-km/h high-speed maglev transportation should be included in the national strategic layout. High-speed maglev trains rely on electromagnetic force to achieve non-contact operation on the track. The suspension system is one of the core components of the maglev vehicle. The faults of suspension systems are inevitable in long-term operation. The types of failure of suspension systems include not only the complete failure of each component, but also partial failure or minor failure caused by performance degradation from extended operation. The occurrence of any kind of failure may affect the stability of the maglev train suspension system, and pose a potential safety hazard during high-speed operation, so it is important to conduct fault-tolerant control (FTC) research on that system.

FTC is a technology that ensures the normal operation of equipment under failures. It was developed in parallel with resolution redundancy-based fault diagnosis techniques (Stoustrup and Blondel, 2004; Benosman and Lum, 2010; Hamayun et al., 2013; Allerhand and Shaked, 2015). There are two categories of FTC. One is passive fault tolerance, which mainly uses the theory of robust control (Ali et al., 2015; Stefanovski, 2018, 2019; Li et al., 2019). This method makes the

✉ Junqi XU, xujunqi@tongji.edu.cn
Yougang SUN, https://orcid.org/0000-0002-1549-0108

Received Mar. 31, 2022; Revision accepted Oct. 6, 2022;
Crosschecked Feb. 16, 2023

redundancy of the system increase with the increasing number of possible failures leading to more conservative control. The other is active fault tolerance (Jin and Yang, 2009; Yetendje et al., 2010; Yang et al., 2012; Gao et al., 2018; Shen et al., 2019; Guo et al., 2020; Li and Wang, 2020; Han et al., 2021a, 2021b), where the fault detection and diagnosis (FDD) module reconfigures the controller or changes the controller structure online when a fault occurs. This method can select the appropriate controller according to the actual situation. However, it is very dependent on the accuracy of fault diagnosis and the effectiveness of the controller switching strategy.

In recent years, many efforts to improve the reliability of suspension systems have been achieved mainly through engineering methods such as increasing system redundancy. For example, to prevent the failures of air gap sensors and sudden changes in gaps at track joints, redundant sets of air gap sensors are used at each suspension point (Wang, 2019). For the join-structure of high-speed maglev, when a suspension point fails, the adjacent suspension point is used to share the effect of suspension (Luo, 2020). At present, scholars at home and abroad are conducting research on FTC methods for maglev trains. This research can be summarized as passive and active fault tolerance methods.

For passive fault tolerance, Sung et al. (2004) proposed a passive FTC method suitable for electromagnetic levitation systems for actuator and sensor faults. Li et al. (2008) designed a passive FTC controller for a typical open-loop unstable linear system using a rational function stable factorization method for a join-structure suspension system.

For active fault tolerance, Wang et al. (2021) proposed an FTC strategy to cope with two fault conditions for permanent magnet-electromagnetic suspension (PEMS)-type high-speed maglev trains with join-structure. Fault tolerance strategies based on signal reconstruction and controller switching are adopted respectively. Zhai et al. (2019) analyzed the problem of performance degradation due to sensor failure for join-structures using a modular redundancy strategy and offered an FTC system based on a state observer. Wang et al. (2014) proposed an active FTC strategy based on feedback gain reconstruction for current sensor faults in maglev trains. A fault diagnosis unit based on a state observer is designed to estimate the output of the current sensor and the diagnosis results are then used to switch the control strategy. Long et al. (2010) studied the electromagnet fault diagnosis and FTC strategies in suspension systems, proposing a method for equating the effect of actuator faults on the change of system parameters to control inputs. Wang (2019) proposed a dynamic compensation method and disturbance suppression based on disturbance estimation and feedback linearization for FTC of a single suspension unit in the join-structure of a PEMS-type high-speed maglev train. Chen et al. (2006) designed a reconfiguration controller and a state estimator to solve the problem of FTC of current and acceleration sensor failures in suspension systems. However, that study used a simplified suspension model and a hardware redundancy approach for gap sensor failures without further research on FTC of gap sensor failure. Long et al. (2007) proposed a new modular suspension system and an active FTC method, based on control law reconstruction, to establish mathematical models under different faults and to design the corresponding optimal controllers. The FTC methods described above often require accurate mathematical models for state estimation or controller reconfiguration and, if the mathematical model of the system is not accurate enough, the fault-tolerance performance will be greatly degraded.

Generally, the sensor fault of the suspension system of the high-speed maglev train can be compensated by designing a state observer (Yan and Edwards, 2008; Li et al., 2013; Chen et al., 2022). When the actuator fails completely, the suspension system uses its adjacent actuators to share the suspension effect through the join-structure. Although it is simple, it will increase the cost and energy consumption, reduce the payload of the maglev train, and have low tolerance to faults. In order to solve these problems, this paper will study the adaptive FTC method for the suspension system of a high-speed maglev train in the case of partial loss of actuator effectiveness. The contributions of this paper can be summarized as follows:

(1) The proposed method does not need to know the fault information of the actuator. In the process of FTC, the adaptive compensation control law changes with the occurrence of a system fault and can be reorganized adaptively, which reduces the conservatism of the system.

(2) The proposed nonlinear controller can theoretically ensure the error approaches zero even in the case of partial loss of actuator effectiveness. The design

and stability of the controller are proved without any linearization approximation.

(3) As verified by the experimental results, the proposed method shows superior control performance against partial actuator failure.

The rest of this paper is organized as follows: in Section 2, the dynamic model of a suspension system based on join-structure is established. In Section 3, the types of actuator failures are described. The controller design and the closed-loop stability analysis are described in Section 4. Section 5 gives the experimental results to verify the effect of FTC. The study is concluded in Section 6 with some summarizing remarks.

2 Suspension system modeling based on join-structure

2.1 Analysis of high-speed maglev train structure

The topology of the high-speed maglev train is shown in Fig. 1, in which the suspension system consists of four suspension frames. Each involves four hover frames and eight controllable suspension units. Each hover frame is provided with a support point utilizing air springs. In the high-speed maglev train, the suspension electromagnet is connected end to end through the hover frame to form a flexible suspension structure. The adjacent electromagnets are supported together by the hover frame and form a join-structure with the controller, sensor, and track. The join-structure is decoupled by the mechanical structure; hence, the suspension system can be decomposed into the control problem of the single join-structure. The single join-structure suspension system is the basic unit of the suspension system. Analyzing the dynamic model and dynamic characteristics of the single join-structure is more general than analyzing the multi-module system, therefore in this study, the high-speed maglev train suspension system is simplified into a suspension model

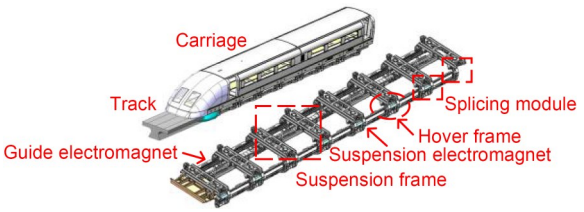

Fig. 1 Schematic diagram of the end carriage of high-speed maglev train

based on the join-structure shown in Fig. 2 to study the FTC problem of the system under partial actuator failure.

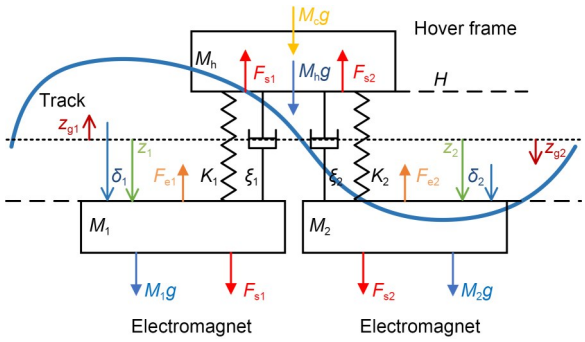

Fig. 2 Schematic diagram of the suspension system based on join-structure

2.2 Suspension model based on join-structure

The operating principle of the maglev train suspension system is that the suspension current is applied to the electromagnet winding coil through the suspension chopper, so that the electromagnet can obtain upward electromagnetic attraction. In the join-structure, the vehicle body is supported by two electromagnets through the hover frame, which is a complex system with multiple inputs and multiple outputs. At the same time, the system has the characteristics of open-loop instability: a strong nonlinear relationship between electromagnetic force and suspension current and a high coupling degree of dynamic equations of the join-structure under two electromagnetic forces. These present a great challenge for the design of an FTC controller. To facilitate the design of an FTC controller, the following reasonable assumptions are made (Li et al., 2017; Zhou et al., 2017; Ding et al., 2019; Sun et al., 2022):

(1) All magnetic flux passes through the air gap between the external poles of the electromagnet (flux leakage is ignored).

(2) Magnetic flux is evenly distributed in the air gap (edge effect is ignored).

(3) The electromagnetic force is assumed to be concentrated at the center point of the electromagnet and its center point coincides with the center of mass.

As shown in Fig. 2, the suspension system based on join-structure is composed of a hover frame, a track, and two suspension electromagnets on the left and right, where two electromagnets are connected to the

hover frame through the Belleville springs that can be regarded as the spring dampers. In the following, subscripts 1 and 2 refer to the physical quantities on the left and right sides, respectively. The vertical downward direction is selected as the positive direction and the lower surface of the track as the reference plane. The irregularity of the track is considered. H is set as the displacement of the hover frame; g as the acceleration of gravity; M_h as the mass of the hover frame; M_c as the mass of the carriage; M_1, M_2 as the masses of the electromagnet on the left and right sides, respectively; F_{e1}, F_{e2} as the electromagnetic forces received by the left and right electromagnets, respectively; K_1, K_2 as the stiffness of the left and right springs, respectively; ξ_1, ξ_2 as the damping coefficients on the left and right sides, respectively; F_{s1}, F_{s2} as the spring forces on the left and right electromagnets, respectively; z_1, z_2 as the displacements of the left and right electromagnets relative to the reference plane, respectively; δ_1, δ_2 as the gaps between the electromagnet and the track under the irregularity of the track; z_{g1}, z_{g2} as the displacements of the track under the irregularity of the track. The relationship for each displacement can be obtained as

$$\begin{cases}\delta_1 = z_1 - z_{g1}, \\ \delta_2 = z_2 - z_{g2}.\end{cases} \tag{1}$$

2.3 Electrical and electromagnetic force equations of the suspension system

It is assumed that the electromagnetic attraction between the electromagnet and the track is F_e, the number of turns of the electromagnet coil is N_e, the effective polar area of an electromagnet is A_e, the air permeability is μ_0, the current in the solenoid coil and the voltage at both ends are respectively i and u, and the resistance of the electromagnet coil is R. The detailed derivation procedure is provided in the electronic supplementary materials (ESM). The electromagnetic force equation and voltage equation can be obtained as

$$F_e = -\frac{\mu_0 N_e^2 A_e}{4}\left(\frac{i}{\delta}\right)^2, \tag{2}$$

$$u = Ri + \frac{\mu_0 N_e^2 A_e}{2\delta}\dot{i} - \frac{\mu_0 N_e^2 A_e i}{2\delta^2}\dot{\delta}. \tag{3}$$

The resulting electrical equation for the left electromagnet is

$$u_1 = R_1 i_1 + \frac{\mu_0 N_{e1}^2 A_{e1}}{2\delta_1}\dot{i}_1 - \frac{\mu_0 N_{e1}^2 A_{e1} i_1}{2\delta_1^2}\dot{\delta}_1. \tag{4}$$

The voltage equation of the right electromagnet is similar, and is not specifically written here. The following equations are introduced with the left electromagnet as an example, and all the derivation can be found in the ESM.

2.4 Dynamic equations for suspension system based on join-structure

The force on the electromagnet by the spring dampers is given by

$$F_{s1} = K_1(H - z_1) + \xi_1\left(\dot{H} - \dot{z}_1\right). \tag{5}$$

Thus, the kinetic equation for the electromagnet can be obtained as

$$M_1\ddot{z}_1 = M_1 g - F_{e1} + F_{s1}. \tag{6}$$

The hover frame is subject to the spring forces on both sides, its own gravity, and the downward force generated by the body of the vehicle through the air springs, so that the kinetic equation is

$$M_h\ddot{H} = M_h g - F_{s1} - F_{s2} + M_c g. \tag{7}$$

2.5 Non-linear model for suspension system based on join-structure

We define the system state variables $\boldsymbol{X}$, output variables $\boldsymbol{Y}$, and control variables $\boldsymbol{u}$:

$$\begin{cases}\boldsymbol{X} = [x_1 \quad x_2 \quad x_3 \quad x_4 \quad x_5 \quad x_6 \quad x_7 \quad x_8]^{\mathrm{T}} = \\ \qquad \left[z_1 \quad \dot{z}_1 \quad i_1 \quad z_2 \quad \dot{z}_2 \quad i_2 \quad H \quad \dot{H}\right]^{\mathrm{T}}, \\ \boldsymbol{Y} = [z_1 \quad z_2]^{\mathrm{T}}, \\ \boldsymbol{u} = [u_1 \quad u_2]^{\mathrm{T}}.\end{cases} \tag{8}$$

The state space expression of the suspension system based on join-structure can be obtained as

$$\begin{cases}\dot{x}_1=x_2,\\ \dot{x}_2=g-\dfrac{\mu_0 N_{e1}^2 A_{e1}}{4M_1}\dfrac{x_3^2}{\delta_1^2}+\dfrac{K_1}{M_1}(x_7-x_1)+\dfrac{\xi_1}{M_1}(x_8-x_2),\\ \dot{x}_3=\dfrac{x_2x_3}{\delta_1}+\dfrac{2\delta_1}{\mu_0 N_{e1}^2 A_{e1}}(u_1-x_3),\\ \dot{x}_4=x_5,\\ \dot{x}_5=g-\dfrac{\mu_0 N_{e2}^2 A_{e2}}{4M_2}\dfrac{x_6^2}{\delta_2^2}+\dfrac{K_2}{M_2}(x_7-x_4)+\dfrac{\xi_2}{M_2}(x_8-x_5),\\ \dot{x}_6=\dfrac{x_5x_6}{\delta_2}+\dfrac{2\delta_2}{\mu_0 N_{e2}^2 A_{e2}}(u_2-x_6),\\ \dot{x}_7=x_8,\\ \dot{x}_8=\dfrac{M_h+M_c}{M_h}g+\dfrac{1}{M_h}\big[K_1x_1+\xi_1x_2+K_2x_4+\xi_2x_5-\\ \quad (K_1+K_2)x_7-(\xi_1+\xi_2)x_8\big].\end{cases} \tag{9}$$

2.6 Model simplification for suspension system based on join-structure

The model represented by Eq. (20), while more closely approximating the actual suspension system, has to consider a number of factors that make the study very difficult, so the model first needs to be simplified. Suppose $N_{e1}=N_{e2}=N_e$, $A_{e1}=A_{e2}=A_e$, $K_1=K_2=K_s$. Because of the low damping of the Belleville springs, a damping of zero is assumed here. Two electromagnets influence the movement of the hover frame, but the movement of the hover frame and the lack of relevant sensors to measure its displacement add to the complexity of the controller design. Therefore, the displacement of the hover frame can be considered as the average of the displacements of the electromagnets on both sides, based on the initial deformation due to the self-weight $M_h g$ and load $M_c g$ of the frame.

$$H=\frac{1}{2}(z_1+z_2)+\frac{1}{2K_s}(M_h+M_c)g. \tag{10}$$

In addition, because the chopper can be used to directly control the magnitude of the current during the actual control process, the control variable is reset to current so as to omit the current loop. Also, we redefine the system state variables, i.e.,

$$\begin{aligned}&\boldsymbol{u}=[\,i_1\quad i_2\,]^{\mathrm{T}},\\ &\boldsymbol{X}=[\,x_1\quad x_2\quad x_3\quad x_4\,]^{\mathrm{T}}=[\,z_1\quad \dot{z}_1\quad z_2\quad \dot{z}_2\,]^{\mathrm{T}}.\end{aligned} \tag{11}$$

Then, the simplified state space expression can be obtained as

$$\begin{cases}\dot{x}_1=x_2,\\ \dot{x}_2=g-\dfrac{\mu_0 N_e^2 A_e}{4M_1}\dfrac{i_1^2}{\delta_1^2}+\dfrac{K_s}{2M_1}(x_3-x_1)+\dfrac{M_h+M_c}{2M_1}g,\\ \dot{x}_3=x_4,\\ \dot{x}_4=g-\dfrac{\mu_0 N_e^2 A_e}{4M_2}\dfrac{i_2^2}{\delta_2^2}+\dfrac{K_s}{2M_2}(x_1-x_3)+\dfrac{M_h+M_c}{2M_2}g.\end{cases} \tag{12}$$

3 Analysis of partial failures

The various parts of the suspension system including actuators, sensors, and controlled objects may fail. In the actual system, because the actuator works in a strong electromagnetic environment, it is the most vulnerable part of the suspension control system. General types of actuator faults include partial or complete failure, current value jamming faults, saturation faults, and floating faults.

The definitions of the actuator faults for the system are described below.

The suspension system can be written in the following affine nonlinear form:

$$\dot{\boldsymbol{x}}=\boldsymbol{f}(\boldsymbol{x})+\boldsymbol{g}(\boldsymbol{x})\boldsymbol{u}, \tag{13}$$

where $\boldsymbol{x}$ is the state of the suspension system, $\boldsymbol{f}(\boldsymbol{x})$ and $\boldsymbol{g}(\boldsymbol{x})$ are the continuous functions, and $\boldsymbol{u}=[u_1, u_2, \cdots, u_i, \cdots, u_n]^{\mathrm{T}}$ denotes the control inputs. The form of faults of the jth actuator can be expressed as

$$u_j=\varpi_j u_{cj}+\bar{u}_j, \tag{14}$$

where u_j is the actual output of the jth actuator, u_{cj} is the ideal control input for the jth actuator, $0\leqslant\varpi_j\leqslant 1$ represents the degree of a partial or total actuator failure, and $\bar{u}_j$ is the control quantity of the stuck fault of the jth actuator. In Eq. (14), this study focuses on the case of partial failure of the actuator with the modeled parameters shown below:

$$0<\varpi_j<1,\quad \bar{u}_j=0. \tag{15}$$

This study mainly studies the adaptive fault tolerance for partial actuator failure, designs the adaptive compensation control law, and uses the effective

actuator to track the target suspension trajectory when the actuator has partial failure, while maintaining good dynamic and steady-state performance.

4 Fault tolerant controller design

4.1 Control object

The control plant can be described in Eq. (12) with partial actuator failure in Eq. (14). The desired air gap is denoted by x_d. The control object of the suspension system of the high-speed maglev train is to maintain the air gap δ_j at the target regardless of partial actuator failure while running. In order to quantitatively describe the control objective, the error signals e are defined as follows:

$$\begin{cases} e_1 = x_1 - x_d, \\ e_2 = x_3 - x_d, \end{cases} \begin{cases} \dot{e}_1 = \dot{x}_1 - \dot{x}_d, \\ \dot{e}_2 = \dot{x}_3 - \dot{x}_d, \end{cases} \begin{cases} \ddot{e}_1 = \ddot{x}_1 - \ddot{x}_d, \\ \ddot{e}_2 = \ddot{x}_3 - \ddot{x}_d. \end{cases} \tag{16}$$

Assumption 1: x_d, $\dot{x}_d$, and $\ddot{x}_d$ satisfy these conditions: x_d, $\dot{x}_d$, $\ddot{x}_d \in L_\infty$, i.e., x_d, $\dot{x}_d$, and $\ddot{x}_d$ are bounded. $|\ddot{x}_d| \leqslant g$ (Sun et al., 2017).

Based on Eqs. (12) and (16), the error systems of the left electromagnet can be derived as follows:

$$M_1 \ddot{e}_1 = M_1 g + \frac{K_s(x_3 - x_1)}{2} + \frac{(M_h + M_c)g}{2} - F_{e1} - \ddot{x}_d. \tag{17}$$

These are controllable electromagnetic forces, i.e., the actual outputs of the actuator. i_1, i_2 are the fault-tolerant suspension control currents of the left and right suspension electromagnets, respectively. Consider the above second failure mode of actuator, i.e.,

$$F_{e1} = \varpi_1 F_{ce1},\ F_{e2} = \varpi_2 F_{ce2}, \tag{18}$$

where F_{e1}, F_{e2} are the actual outputs of the left and right actuators, respectively. F_{ce1}, F_{ce2} are the ideal control inputs of the left and right actuators, respectively. ϖ_1, $\varpi_2 \in (0, 1]$ denote the failure degrees of the left and right actuators, respectively.

First, the suspension controller of the left electromagnet module is designed. The sliding surface of the left electromagnet s_1 is as follows:

$$s_1 = c_1 e_1 + \dot{e}_1, \tag{19}$$

where c_1 is the parameter of sliding mode control to regulate the speed, at which the state converges to zero, and $c_1 > 0$.

Setting $\varphi_1 = \varpi_1 / M_1$, $\xi_1 = 1/\varphi_1$. The FTC law of the left electromagnet module is designed as follows:

$$i_1(t) = \left[\frac{1}{\kappa_1} \delta_1^2 \hat{\xi}_1 \left(k_{t1} s_1 + c_1 \dot{e}_1 + g + \frac{K_s(x_3 - x_1)}{2M_1} + \frac{(M_h + M_c)}{2M_1} g - \ddot{x}_d \right) \right]^{\frac{1}{2}}, \tag{20}$$

where $\kappa_1 = \mu_0 N_{e1}^2 A_{e1}/4$, $k_{t1} > 0$ are the fault tolerance control coefficients. $\hat{\xi}_1$ is an adaptive estimate value containing fault information for the left module, which can be determined by the following adaptive update law:

$$\dot{\hat{\xi}}_1 = \lambda_1 s_1 \left(k_{t1} s_1 + c_1 \dot{e}_1 + g + \frac{K_s(x_3 - x_1)}{2M_1} + \frac{(M_h + M_c)}{2M_1} g - \ddot{x}_d \right) \mathrm{sgn}(\varphi_1), \tag{21}$$

where $\lambda_1 > 0$ denotes adaptive gain.

Thus, $\mathrm{sgn}(\varphi_1) = \mathrm{sgn}\left(1/M_1\right)$.

The sliding mode surface and control law of the right electromagnet can be obtained similarly, see the ESM for details.

4.2 Closed-loop stability analysis

Before proceeding to the stability analysis, the extended Barbalat lemma is first presented, and will be used in the following analysis.

Extended Barbalat lemma: $x:[0, \infty) \to \mathbb{R}$ is square integrable and $\mathbb{R}$ is the domain of real numbers, i.e., $\lim\limits_{t \to \infty} \int_0^t x^2(\tau)\,\mathrm{d}\tau < \infty$. If $x(t)$ is uniformly continuous, then $\lim\limits_{t \to \infty} x(t) = 0$.

The closed-loop stability analysis of the proposed control law under partial actuator failure is carried out below. For the suspension system based on join-structure with two suspension electromagnets, we obtain:

Theorem 1: The designed adaptive suspension controller Eq. (20), together with the proposed update mechanism Eq. (21), can also achieve the control objective even if the left actuator has a partial failure in Eq. (18) in the sense that

$$\begin{aligned}&\lim_{t\to\infty} e_1(t)=0, \quad \lim_{t\to\infty}\dot{e}_1(t)=0,\\&\lim_{t\to\infty} e_2(t)=0, \quad \lim_{t\to\infty}\dot{e}_2(t)=0.\end{aligned} \tag{22}$$

The non-negative scalar Lyapunov function V is constructed as follows:

$$V=\frac{1}{2}s_1^2+\frac{|\varphi_1|}{2\lambda_1}\tilde{\xi}_1^2+\frac{1}{2}s_2^2+\frac{|\varphi_2|}{2\lambda_2}\tilde{\xi}_2^2, \tag{23}$$

where $s_1=c_1e_1+\dot{e}_1$, $\tilde{\xi}_1=\hat{\xi}_1-\xi_1$, $\lambda_1>0$, $s_2=c_2e_2+\dot{e}_2$, $\tilde{\xi}_2=\hat{\xi}_2-\xi_2$, and $\lambda_2>0$.

Taking the derivative of both sides of Eq. (23) with respect to time, and setting

$$\begin{aligned}\gamma_1&=k_{t1}s_1+c_1\dot{e}_1+g+\frac{K_s(x_3-x_1)}{2M_1}+\frac{(M_h+M_c)}{2M_1}g-\ddot{x}_d,\\\gamma_2&=k_{t2}s_2+c_2\dot{e}_2+g+\frac{K_s(x_1-x_3)}{2M_2}+\frac{(M_h+M_c)}{2M_2}g-\ddot{x}_d.\end{aligned} \tag{24}$$

The following equation can be obtained through simplification (the specific derivation process is included in the ESM):

$$\begin{aligned}\dot{V}=&s_1\left(\gamma_1-k_{t1}s_1-\varphi_1\hat{\xi}_1\gamma_1\right)+\varphi_1\tilde{\xi}_1s_1\gamma_1+\\&s_2\left(\gamma_2-k_{t2}s_2-\varphi_2\hat{\xi}_2\gamma_2\right)+\varphi_2\tilde{\xi}_2s_2\gamma_2=\\&s_1(\gamma_1-k_{t1}s_1-\varphi_1\xi_1\gamma_1)+s_2(\gamma_2-k_{t2}s_1-\varphi_1\xi_1\gamma_1)=\\&-k_{t1}s_1^2-k_{t2}s_2^2\leqslant 0.\end{aligned} \tag{25}$$

Because $V\geqslant 0$ and $\dot{V}\leqslant 0$ are based on the Lyapunov method, we can conclude that V is bounded.

It can be obtained from $\dot{V}=-k_{t1}s_1^2-k_{t2}s_2^2$ that:

$$\int_0^t\dot{V}\mathrm{d}t=-k_{t1}\int_0^t s_1^2\mathrm{d}t-k_{t2}\int_0^t s_2^2\mathrm{d}t, \tag{26}$$

i.e., $V(\infty)-V(0)=-k_{t1}\int_0^\infty s_1^2\mathrm{d}t-k_{t2}\int_0^t s_2^2\mathrm{d}t$.

While $t\to\infty$, because $V(\infty)$ is bounded, then $\int_0^\infty s_1^2\mathrm{d}t$ and $\int_0^t s_2^2\mathrm{d}t$ are bounded, respectively, i.e., s_1 and s_2 are square integrable, respectively. Thus, it is easy to know that s_1 and s_2 are uniformly continuous. Based on the above extended Barbalat lemma, while $t\to\infty$, $\lim_{t\to\infty}s_1=0$ and $\lim_{t\to\infty}s_2=0$. Since $s_1=c_1e_1+\dot{e}_1$, $s_2=c_2e_2+\dot{e}_2$, $c_1\neq 0$, and $c_2\neq 0$, we have $\lim_{t\to\infty}e_1(t)=0$, $\lim_{t\to\infty}\dot{e}_1(t)=0$, $\lim_{t\to\infty}e_2(t)=0$, and $\lim_{t\to\infty}\dot{e}_2(t)=0$. Thus, the closed-loop system with the proposed control law is asymptotically stable.

Remark 1: The proposed adaptive FTC controller makes use, in part, of adaptive techniques, which can use the state feedback information with partial actuator failure to readjust the controller parameters after the fault occurs so as to stabilize the system again. Moreover, different from the traditional linear matrix inequality (LMI)-based suspension FTC controller, there is no linearization approximation in the process of controller design and stability analysis.

5 Experimental results

To show the effectiveness of the proposed adaptive FTC method, a series of experiments are carried out on a high-speed maglev vehicle-rail magnetic coupling experiment platform exhibiting join-structure of two electromagnets, as shown in Fig. 3. The specific composition of each part of the experiment platform is shown in the ESM. The experiment platform is connected with dSPACE, which can be controlled by MATLAB/Simulink in real-time (Xu et al., 2021). The experiment platform includes a hydraulic excitation device, join-structure with Belleville springs, left and right electromagnet modules, suspension sensors, suspension control boxes, dSPACE, air springs, and a rail bracket. The suspension control algorithm can be overlapped on the dSPACE simulation platform.

Fig. 3 High-speed maglev vehicle-rail magnetic coupling experiment platform

Throughout the experiments, the physical parameters for the experiment platform are set to be: $M_1=M_2=350$ kg, $M_h+M_c=2100$ kg, $K_s=1.236\times10^7$ N/m, $\kappa_1=\kappa_2=0.004$, and $g=9.8$ m/s^2. The control gains for

the proposed adaptive FTC controller Eqs. (19) and (20) are selected as $k_{t1}=k_{t2}=200$, $c_1=c_2=500$, and $\lambda_1=\lambda_2=4000$. The initial value of the suspension air gap is $x_{10}=x_{30}=0.02$ m. To demonstrate the effects of the proposed controller dealing with partial actuator failure in Case 2 of the following two experiments, we also compared the proposed control method with a passive FTC controller, for which control gains are calculated by the LMI method (Long et al., 2008). The passive FTC controller can be expressed as follows (Zhang and Gong, 2018):

$$\boldsymbol{U}_{\mathrm{F}}=\boldsymbol{K}_{\mathrm{f}}\begin{bmatrix}k_{\mathrm{p1}}x_1 & k_{\mathrm{d1}}x_2\\ k_{\mathrm{p2}}x_1 & k_{\mathrm{d2}}x_2\end{bmatrix}, \tag{27}$$

where $\boldsymbol{U}_{\mathrm{F}}$ is the control quantity of actuator; $\boldsymbol{K}_{\mathrm{f}}$ is the state feedback coefficient of fault-tolerant control; k_{p} and k_{d} are both control gains.

Through offline calculation based on LMI, we select $\boldsymbol{K}_{\mathrm{f}}$=[1233.1 897].

Next, two sets of experiments are implemented.

5.1 Experiment 1: static levitation

In this group of experiments the target air gap $x_{\mathrm{d}}=0.012$ m. To facilitate the observation, we only target partial failure of the left electromagnet in the experiments.

5.1.1 Case 1: without actuator failure (normal condition)

When there is no actuator failure in the system, the electromagnet is suspended from the initial position to the target position starting from 2 s. The experimental results of the air gap response and control current response of the left electromagnet with the proposed FTC are shown in Figs. 4 and 5.

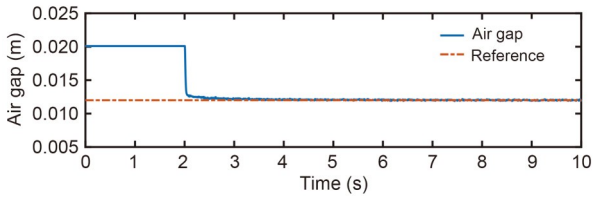

Fig. 4 Air gap tracking response in normal condition (static levitation without actuator failure)

5.1.2 Case 2: with partial actuator failure

In the normal suspension state, a partial failure of the left actuator is introduced at 5 s, i.e., $\varpi_1=0.5$. The experimental results with the traditional passive FTC of the left electromagnet are shown in Figs. 6 and 7. The experimental results with the proposed FTC are shown in Figs. 8 and 9. The adaptation gain $\hat{\xi}_1$ is shown in Fig. 10.

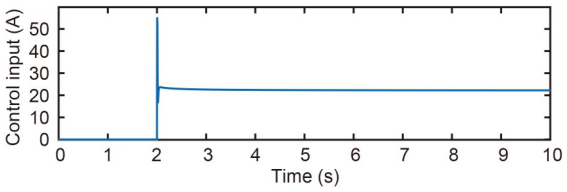

Fig. 5 Control current response in normal condition (static levitation without actuator failure)

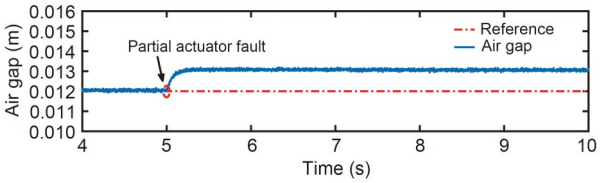

Fig. 6 Passive FTC: air gap response with partial actuator failure ($\varpi_1=0.5$)

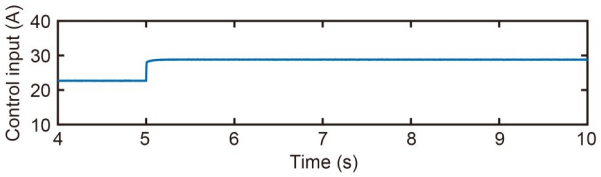

Fig. 7 Passive FTC: current response with partial actuator failure ($\varpi_1=0.5$)

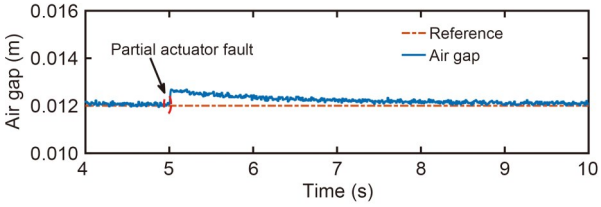

Fig. 8 Proposed FTC: air gap response with partial actuator failure ($\varpi_1=0.5$)

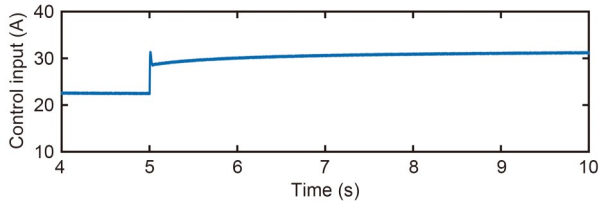

Fig. 9 Proposed FTC: current response with partial actuator failure ($\varpi_1=0.5$)

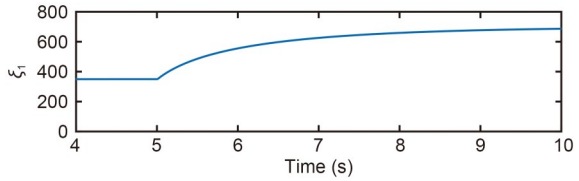

Fig. 10 Proposed FTC: adaptation gain $\hat{\xi}_1$ ($\varpi_1=0.5$)

5.2 Experiment 2: trajectory tracking

Most of the maglev track is not absolutely smooth, so it is very important to investigate the tracking performance of the proposed suspension controller. Here it is assumed that the target air gap to be tracked is $x_d=0.012+0.002\sin(2t)$ (m).

5.2.1 Case 1: without actuator failure (normal condition)

When there is no actuator failure in the system, the electromagnet tracks the uneven trajectory from its initial position starting at 2 s. The experimental results of the air gap response and control current response of the left electromagnet with proposed FTC are shown in Figs. 11 and 12.

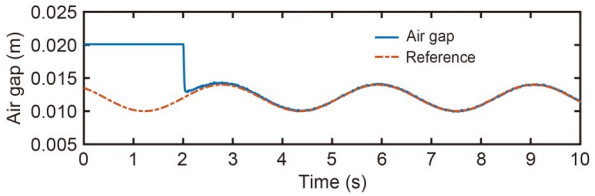

Fig. 11 Air gap tracking response in normal condition (track tracking without actuator failure)

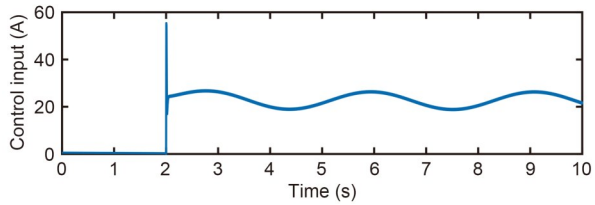

Fig. 12 Control current response in normal condition (track tracking without actuator failure)

5.2.2 Case 2: with partial actuator failure

In normal suspension tracking state, the partial failure of the left actuator is introduced in 5 s, i.e., $\varpi_1=0.5$. The tracking experimental results with the traditional passive FTC of the left electromagnet are shown in Figs. 13 and 14. The tracking experimental results with the proposed FTC are shown in Figs. 15 and 16. The adaptation gain $\hat{\xi}_1$ in this case is shown in Fig. 17.

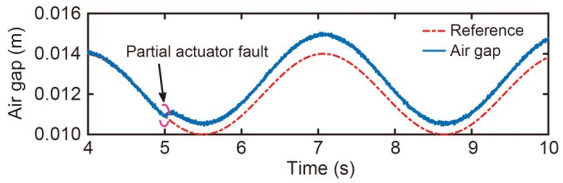

Fig. 13 Passive FTC: air gap tracking response with partial actuator failure ($\varpi_1=0.5$)

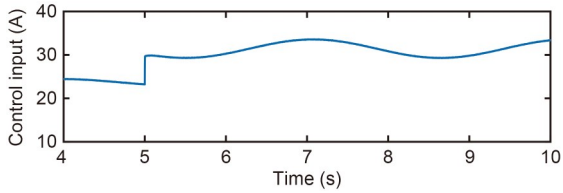

Fig. 14 Passive FTC: tracking current response with partial actuator failure ($\varpi_1=0.5$)

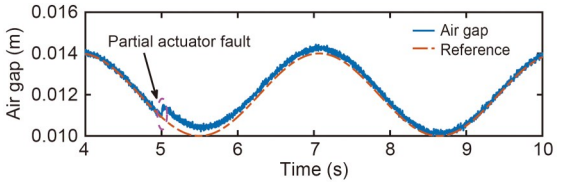

Fig. 15 Proposed FTC: air gap tracking response with partial actuator failure ($\varpi_1=0.5$)

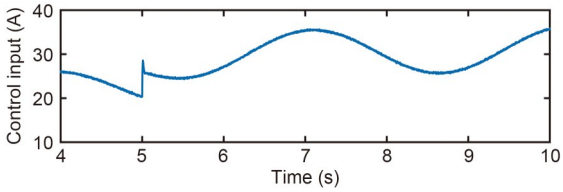

Fig. 16 Proposed FTC: tracking current response with partial actuator failure ($\varpi_1=0.5$)

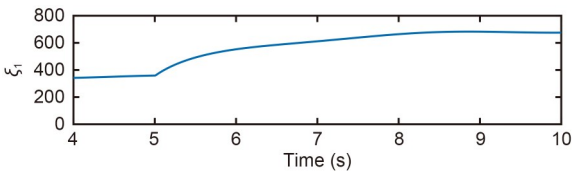

Fig. 17 Proposed FTC: adaptation gain $\hat{\xi}_1$ in Experiment 2 ($\varpi_1=0.5$)

As can be seen from Figs. 4 and 5, the proposed suspension controller can reach the target air gap position within 0.5 s without overshooting and the error of the air gap tends to 0. The control current is smooth

and there is no phenomenon of chattering. Also, when a partial failure occurs in the left actuator during the stable suspension, the traditional passive FTC can still maintain the suspension state, but the air gap error is about 9.0% at 5 s in Fig. 6 and cannot eliminate the steady-state error. The proposed controller can quickly eliminate the effect of the failure and generate only a 5.5% error of the suspension air gap at 5 s in Fig. 8, followed by a gradual convergence of the error tending to 0. As can be seen from Figs. 11 and 12, when there is no actuator failure, the proposed suspension controller can track the irregular trajectory well, and the error of the air gap tends to 0 within 1.1 s after the suspension instruction is issued. The control current is relatively smooth without the phenomenon of chattering. Also, when a partial failure occurs in the left actuator during the stable suspension, the traditional passive FTC can track the target trajectory roughly, but the air gap error is about 7.8% at 5 s in Fig. 13 and cannot eliminate the tracking error obviously. The proposed controller generates a 7.1% error of the suspension air gap at 5 s in Fig. 15. The proposed controller can quickly eliminate the effect of the actuator failure, and the error of the suspension air gap basically tends to 0 at 9 s. It can be seen that the proposed controller can compensate for the effect of partial actuator failure effectively while suspending and tracking faster than the traditional passive FTC.

6 Conclusions

This study proposes a non-linear FTC strategy with adaptive compensation which achieves superior performance in suspension control under partial actuator failure without fault diagnosis and isolation. To our knowledge, this is the first FTC method that can both asymptotically and stably regulate and track the target trajectory subject to partial actuator failure with the least assumptions (e.g., linearization approximation). The contribution is both theoretically and practically important. Theoretically, the derived FTC law is simple in structure and the control law can change adaptively with the occurrence of faults, thus improving the reliability and transient performance of the suspension system. Through rigorous mathematical analysis, we demonstrate that the entire closed-loop system is globally asymptotically stable, i.e., the error of the air gap is theoretically shown to converge to zero without the approximation/linearization of the original non-linear dynamic whereas the existing methods of tolerant control of suspension systems assume that the system state is sufficiently close to the equilibrium point. The experimental results show that the method can indeed compensate for partial actuator failure in practice, while achieving regular suspension control or tracking suspension control, and which has good robustness. Our future research will be devoted to the application of the full-scale high-speed maglev train suspension system in the National Maglev Transportation Engineering R&D Center.

Acknowledgments

This work is supported by the National Natural Science Foundation of China (Nos. 52272374 and 52072269), the Shanghai Soft Science Research Project (No. 22692194800), and the Fundamental Research Funds for the Central Universities, China.

Author contributions

Yougang SUN designed the research and controller design. Fengxing LI and Zhenyu HE designed the hardware experiment and processed the corresponding data. Guobin LIN implemented the modeling process. Junqi XU performed the stability demonstration. Zhenyu HE collected and analyzed the literature.

Conflict of interest

Yougang SUN, Fengxing LI, Guobin LIN, Junqi XU, and Zhenyu HE declare that they have no conflict of interest.

References

Ali SA, Guermouche M, Langlois N, 2015. Fault-tolerant control based super-twisting algorithm for the diesel engine air path subject to loss-of-effectiveness and additive actuator faults. *Applied Mathematical Modelling*, 39(15):4309-4329. https://doi.org/10.1016/j.apm.2014.12.047

Allerhand LI, Shaked U, 2015. Robust switching-based fault tolerant control. *IEEE Transactions on Automatic Control*, 60(8):2272-2276. https://doi.org/10.1109/TAC.2014.2375752

Benosman M, Lum KY, 2010. Passive actuators' fault-tolerant control for affine nonlinear systems. *IEEE Transactions on Control Systems Technology*, 18(1):152-163. https://doi.org/10.1109/TCST.2008.2009641

Boldea I, Tutelea LN, Xu W, et al., 2018. Linear electric machines, drives, and maglevs: an overview. *IEEE Transactions on Industrial Electronics*, 65(9):7504-7515. https://doi.org/10.1109/TIE.2017.2733492

Chen C, Xu JQ, Rong LJ, et al., 2022. Neural-network-state-observation-based adaptive inversion control method of

maglev train. *IEEE Transactions on Vehicular Technology*, 71(4):3660-3669. https://doi.org/10.1109/TVT.2022.3142144

Chen HX, Long ZQ, Chang WS, 2006. Fault tolerant control research for high-speed maglev system with sensor failure. The 6th World Congress on Intelligent Control and Automation, p.2281-2285. https://doi.org/10.1109/WCICA.2006.1712766

Ding JF, Yang X, Long ZQ, 2019. Structure and control design of levitation electromagnet for electromagnetic suspension medium-speed maglev train. *Journal of Vibration and Control*, 25(6):1179-1193. https://doi.org/10.1177/1077546318813405

Fang YT, Yao YY, 2007. Dynamic performance analysis model of high-reliability EMS-maglev system. *Journal of Zhejiang University-SCIENCE A*, 8(3):412-415. https://doi.org/10.1631/jzus.2007.A0412

Gao ZF, Cheng P, Qian MS, et al., 2018. Active fault-tolerant control approach design for rigid spacecraft with multiple actuator faults. *Proceedings of the Institution of Mechanical Engineers, Part I: Journal of Systems and Control Engineering*, 232(10):1365-1378. https://doi.org/10.1177/0959651818782847

Guo G, Li P, Hao LY, 2020. Adaptive fault-tolerant control of platoons with guaranteed traffic flow stability. *IEEE Transactions on Vehicular Technology*, 69(7):6916-6927. https://doi.org/10.1109/TVT.2020.2990279

Hamayun MT, Edwards C, Alwi H, 2013. A fault tolerant control allocation scheme with output integral sliding modes. *Automatica*, 49(6):1830-1837. https://doi.org/10.1016/j.automatica.2013.02.043

Han KZ, Chen CZ, Chen MD, et al., 2021a. Constrained active fault tolerant control based on active fault diagnosis and interpolation optimization. *Entropy*, 23(8):924. https://doi.org/10.3390/e23080924

Han KZ, Feng J, Zhao Q, et al., 2021b. Robust constrained predictive fault-tolerant control with generalized input parameterization and event-triggered regulation: design and experimental results. *IEEE Transactions on Industrial Electronics*, 68(9):8615-8625. https://doi.org/10.1109/TIE.2020.3013521

Jin XZ, Yang GH, 2009. Robust adaptive fault-tolerant compensation control with actuator failures and bounded disturbances. *Acta Automatica Sinica*, 35(3):305-309. https://doi.org/10.1016/S1874-1029(08)60079-8

Lee HW, Kim KC, Lee J, 2006. Review of maglev train technologies. *IEEE Transactions on Magnetics*, 42(7):1917-1925. https://doi.org/10.1109/TMAG.2006.875842

Li N, Sun HY, Zhang QL, 2019. Robust passive adaptive fault tolerant control for stochastic wing flutter via delay control. *European Journal of Control*, 48:74-82. https://doi.org/10.1016/j.ejcon.2019.04.008

Li XL, Zhang ZZ, Long ZQ, et al., 2008. Fault-tolerant control for maglev train with joint-structure based on simultaneous stablization. *Control Engineering of China*, 15(6):724-727 (in Chinese). https://doi.org/10.3969/j.issn.1671-7848.2008.06.028

Li XL, Zhai MD, Hao AM, 2017. Maglev train suspension control parameters optimization based on output saturation. *Journal of National University of Defense Technology*, 39(4):149-153 (in Chinese). https://doi.org/10.11887/j.cn.201704023

Li XY, Wang JZ, 2020. Active fault-tolerant consensus control of Lipschitz nonlinear multiagent systems. *International Journal of Robust and Nonlinear Control*, 30(13):5233-5252. https://doi.org/10.1002/rnc.5057

Li Y, Li J, Zhang G, et al., 2013. Disturbance decoupled fault diagnosis for sensor fault of maglev suspension system. *Journal of Central South University*, 20(6):1545-1551. https://doi.org/10.1007/s11771-013-1646-0

Long ZQ, Xue S, Zhang ZZ, et al., 2007. A new strategy of active fault-tolerant control for suspension system of maglev train. IEEE International Conference on Automation and Logistics, p.88-94. https://doi.org/10.1109/ICAL.2007.4338536

Long ZQ, Xue S, Chen HX, 2008. Passive fault tolerant control for suspension system of Maglev train based on LMI. *Computer Simulation*, 25(2):265-268 (in Chinese). https://doi.org/10.3969/j.issn.1006-9348.2008.02.069

Long ZQ, Li Y, He G, 2010. Research on electromagnet fault diagnosis technology of suspension control system of maglev train. *Control and Decision*, 25(7):1004-1009 (in Chinese). https://doi.org/10.13195/j.cd.2010.07.47.longzhq.017

Luo J, 2020. Research on Fault Diagnosis Method of Suspension System of High Speed Maglev Train. MS Thesis, National University of Defense Technology, Changsha, China (in Chinese). https://doi.org/10.27052/d.cnki.gzjgu.2020.000199

Shen Q, Yue CF, Goh CH, et al., 2019. Active fault-tolerant control system design for spacecraft attitude maneuvers with actuator saturation and faults. *IEEE Transactions on Industrial Electronics*, 66(5):3763-3772. https://doi.org/10.1109/TIE.2018.2854602

Stefanovski JD, 2018. Passive fault tolerant perfect tracking with additive faults. *Automatica*, 87:432-436. https://doi.org/10.1016/j.automatica.2017.09.011

Stefanovski JD, 2019. Fault tolerant control of descriptor systems with disturbances. *IEEE Transactions on Automatic Control*, 64(3):976-988. https://doi.org/10.1109/TAC.2018.2827702

Stoustrup J, Blondel VD, 2004. Fault tolerant control: a simultaneous stabilization result. *IEEE Transactions on Automatic Control*, 49(2):305-310. https://doi.org/10.1109/TAC.2003.822999

Sun N, Fang YC, Chen H, 2017. Tracking control for magnetic-suspension systems with online unknown mass identification. *Control Engineering Practice*, 58:242-253. https://doi.org/10.1016/j.conengprac.2016.09.003

Sun YG, Xu JQ, Lin GB, et al., 2022. RBF neural network-based supervisor control for maglev vehicles on an elastic track with network time delay. *IEEE Transactions on Industrial Informatics*, 18(1):509-519. https://doi.org/10.1109/TII.2020.3032235

Sung HK, Kim DS, Cho HJ, et al., 2004. Fault tolerant control of electromagnetic levitation system. Proceedings of the 18th Magnetically Levitated System and Linear Drives

Conference, p.676-688.

Wang ZQ, 2019. Fault Diagnosis and Tolerant Control for High Speed Maglev Train Suspension System. PhD Thesis, National University of Defense Technology, Changsha, China (in Chinese). https://doi.org/10.27052/d.cnki.gzjgu.2019.000022

Wang ZQ, Li XL, Wang QZ, 2014. Current sensor active fault tolerance control based on feedback gain reconfiguration. *Applied Mechanics and Materials*, 511-512:1012-1016. https://doi.org/10.4028/www.scientific.net/AMM.511-512.1012

Wang ZQ, Long ZQ, Li XL, 2019. Fault analysis and tolerant control for high speed PEMS maglev train end joint structure with disturbance rejection. *Journal of Electrical Engineering & Technology*, 14(3):1357-1366. https://doi.org/10.1007/s42835-019-00141-w

Wang ZQ, Long ZQ, Li XL, 2021. Fault tolerant control for joint structure in PEMS high speed maglev train. *Asian Journal of Control*, 23(1):486-498. https://doi.org/10.1002/asjc.2320

Xu JQ, Lin GB, Chen C, et al., 2021. A Simulation Platform of Suspension Control for High Speed and Medium and Low Speed Maglev Train. CN Patent CN111103809B (in Chinese).

Yan XG, Edwards C, 2008. Adaptive sliding-mode-observer-based fault reconstruction for nonlinear systems with parametric uncertainties. *IEEE Transactions on Industrial Electronics*, 55(11):4029-4036. https://doi.org/10.1109/TIE.2008.2003367

Yang H, Zhang KP, Wang X, 2012. Multi-model switching predictive control with active fault tolerance for high-speed train. *Control Theory & Applications*, 29(9):1211-1214 (in Chinese).

Yetendje A, Seron MM, Doná JAD, et al., 2010. Sensor fault-tolerant control of a magnetic levitation system. *International Journal of Robust and Nonlinear Control*, 20(18):2108-2121. https://doi.org/10.1002/rnc.1572

Zhai MD, Long ZQ, Li XL, 2019. Fault-tolerant control of magnetic levitation system based on state observer in high speed maglev train. *IEEE Access*, 7:31624-31633. https://doi.org/10.1109/ACCESS.2019.2898108

Zhang LP, Gong DL, 2018. Passive fault-tolerant control for vehicle active suspension system based on H_2/H_∞ approach. *Journal of Vibroengineering*, 20(4):1828-1849. https://doi.org/10.21595/jve.2017.18264

Zhou DF, Yu PC, Wang LC, et al., 2017. An adaptive vibration control method to suppress the vibration of the maglev train caused by track irregularities. *Journal of Sound and Vibration*, 408:331-350. https://doi.org/10.1016/j.jsv.2017.07.037

Electronic supplementary materials

Sections S1–S3